


A Deep-Learning-Based Fusion Approach for Global Cyclone Detection Using Multiple Remote Sensing Data

Ming Xie , Member, IEEE, Ying Li, and Shuang Dong

Abstract—Cyclone detection is a classic yet developing topic. Various methods have been developed for the purpose of cyclone detection based on sea level pressure, cloud imagery, and wind field. In this article, a data fusion approach that utilizes the data productions from multiple remote sensors is presented. A deep-learning-based object detection algorithm was adopted to form a global-scale cyclone detection model. Wind field data obtained from mean wind field-advanced scatterometer was integrated with the rainfall intensity data obtained from global precipitation measurement as the dataset for model training and testing. Feature pyramid network (FPN), which was designed for small target detection, was integrated with faster-regions with convolutional neural network to detect the cyclones within the fused dataset. The proposed model consists of two modules: a feature extractor and region proposal network based on FPN that searches for the potential areas of cyclones within the fused dataset, and a regions of interests processor that calibrate the locations of cyclone regions through a fully-connected neural network and a bounding box regression. An ablation experiment was also designed in the study in order to verify the necessity of data fusion. The results from ablation experiment suggested that the wind field data provided more contribution in the cyclone detection than the precipitation data.

Index Terms—Cyclone detection, data fusion, deep learning, precipitation, wind field.

I. INTRODUCTION

CYCLONE is a typical extreme weather condition that negatively affects the safety of maritime transportation and coastal residents. Therefore, cyclone detection is an important topic in the related field. Since 1960s, remote sensing technology has been developed and applied to monitor oceanic environment, including cyclones on the sea surface. Meanwhile, thanks to the improvements in the spatial coverage and resolution of remote sensors, detecting cyclones in large spatial and temporal scales became a trend in relevant studies. Researchers have made attempts to accomplish such objective and their works can be classified as follows based on the data they utilized.

Manuscript received 8 May 2022; revised 5 August 2022 and 29 September 2022; accepted 1 November 2022. Date of publication 7 November 2022; date of current version 14 November 2022. This work was supported in part by the China National Key R&D Program under Grant 2019YFB1600600 and in part by the Liaoning Revitalization Talents Program under Grant XLYC2001002. (Corresponding author: Ming Xie.)

The authors are with the Navigation College, Dalian Maritime University, Dalian 116026, China (e-mail: mingxie@dlnu.edu.cn; yldmu@dlnu.edu.cn; dshdmu@dlnu.edu.cn).

Digital Object Identifier 10.1109/JSTARS.2022.3219809

- 1) Cyclones are characterized as low-pressure centers [1]. Thus, low sea-level pressure (SLP) zone is a classic identifier for the presence of cyclones [2], [3]. By comparing the Laplacian operator of SLP, Simmonds et al. [4] proposed an automatic cyclone detection algorithm. Hanley and Caballero [5] further developed an identification and tracking method for multicenter cyclones by examining the gradient of SLP. Nevertheless, less SLP application is being made for cyclone detection in the recent studies because of the lack of in situ and remote sensing data.
- 2) Because the wind field of cyclone wing is usually characterized as high vorticity zone compared with surrounding area, the remotely sensed wind field data, which is usually obtained through satellite-based scatterometer, have been widely applied in cyclone detection. A classic approach for identifying cyclone in the wind field is the Okubo–Weiss (OW) method, which is proposed to quantitatively evaluate the significance between rotation and deformation in the flow field [6], [7]. The OW parameter W is defined specifically as

$$W = S_s^2 + S_n^2 - \omega^2 \quad (1)$$

where S_s and S_n are the shear and normal components of strain, and ω is the relative vorticity. These parameters can be specifically calculated using

$$S_s = \frac{\partial V'}{\partial x} + \frac{\partial U'}{\partial y}, S_n = \frac{\partial U'}{\partial x} - \frac{\partial V'}{\partial y}, \omega = \frac{\partial V'}{\partial x} - \frac{\partial U'}{\partial y} \quad (2)$$

where U' and V' are the zonal and meridional components of the flow velocity and x and y are the spatial coordinates. Some cyclone detection algorithms have been proposed based on the wind field information derived from remote sensing data and OW parameters [8], [9]. Tory et al. [10] took the product of the normalized OW parameter and the absolute vorticity, and proposed Okubo–Weiss–Zeta predictor (OWZP) to identify the regions of enhanced vorticity with weak deformation in the wind field, based on which they further designed a model-free cyclone detection scheme. The major disadvantage of OW method is that the threshold of OW parameter is only valid in a regional area [11], [12]. Thus, the OW-based cyclone detection methods are usually not capable for cyclone detection in large spatial scale. In order to overcome this shortage, Xie et al. [13] designed a deep-learning-based target detection algorithm and achieved

global-scale cyclone detection using wind field data. The deep learning model was able to recognize the characteristics of vorticity in the wind field, but also reported false alarms including monsoon gyre or other cyclone-like turbulence.

- 3) The infrared (IR) remote sensing images can capture the shapes of cyclone clouds, which have a strong characteristic of geometric symmetry. With the wide application of advanced machine learning algorithms in image processing, automatic cyclone detection using IR images has become a hotspot in recent studies. Lee and Liu [14] classified the shapes of clouds formed by tropical cyclones in remote sensing images into eight categories, based on which they proposed a cyclone detection method using neural networks. Jaiswal and Kishtawal [15], [16] conducted a series of studies on cyclone detection using IR remote sensing images based on spiral template and gradient vectors of brightness temperature. Different method was proposed by Liu et al. [17], who designed an algorithm to detect cyclone's edge using Sobel operator. Xu et al. [18] derived the cloud motion wind (CMW) field from IR images, and proposed a cyclone detection algorithm combining CMW and IR images. Shakya et al. [19] developed a deep-learning-based model using IR imagery and applied it to track the cyclone path in Indian Ocean. Similar methods were proposed to detect cyclone or storm using multispectral images [20], radar images [21], and other earth observations [22]. There have also been sufficient studies that developed the models to estimate cyclone intensities using IR images [23], [24], [25], [26], [27], [28], [29], [30], [31]. However, this topic is considered beyond the scope of this article, and thus will not be discussed in detail here.

As a state-of-the-art data mining technique, data fusion method has become a focus in the researches on remote sensing data processing. Researchers have also made some attempt to identify the presence of cyclone using the datasets obtained from multiple types of remote sensors. Ho and Talukder [32], [33], [34] conducted a series of studies on cyclone detection using multiple remote sensing datasets. They combined the wind field data obtained from quick scatterometer (QuikSCAT) with the precipitation data obtained from tropical rainfall measurement mission (TRMM), and then distinguished the tropical cyclone based on support vector machine. Warunsin and Chitsobhuk [35] combined the wind data with cloud shape and developed a fuzzy inference system for cyclone detection. They claimed that the combined dataset could achieve higher detection accuracy than using wind field data alone. Murata et al. [36] utilized two quantities that derived from the radial gradient and the tangential asymmetry of vortex properties cyclones to build a topological model for tropical cyclone detection. These successful applications indicate that the integrated remote sensing data could potentially be applied to analyze the complex meteorological system, including cyclone detection.

Following the route of remote sensing data fusion, this article presents a cyclone detection model based on deep learning. Wind field and precipitation, which are two types of meteorological features strongly related to the cyclone events, are selected to

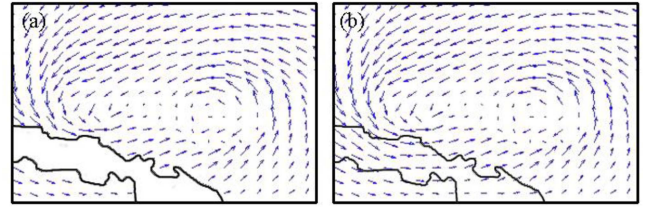


Fig. 1. Wind field vectors over an island. (a) Raw data. (b) Interpolated data.

generate an integrated dataset. And an object detection method based on deep convolutional neural network (CNN) is introduced to identify the cyclones within the integrated dataset. The data fusion approach, deep-learning-based model, and the design of ablation experiment are described in detail in Section II. The cyclone detection results at global and regional scales are presented in Section III. The detection accuracies from ablation experiment and comparison experiment are quantitatively analyzed in Section IV. The potential applications and limitations of the proposed model are also discussed in Section IV. It is expected that the proposed method could provide a novel method for global cyclone detection, and promote the studies on remote sensing data fusion approach.

II. METHODOLOGY

A. Data Acquisition and Processing

Draw on the successful experiences in the studies by Ho and Talukder [33], [34], wind field vectors and precipitation data were applied to the cyclone detection model. The details on data acquisition and processing are discussed as follow.

1) *Wind Field Data*: As mentioned in the introduction, wind field of cyclone events have strong characteristic of vorticity, and wind field data have been applied to detect cyclones in previous studies. The mean wind field (MWF) data used in this article is derived from advanced scatterometer (ASCAT), which is provided by European Remote Sensing program of the European Space Agency. MWF-ASCAT was upgraded from QuikSCAT in term of spatial resolution: it covers the wind field data on the sea surface between 80°N - 80°S and 180°W - 0° - 180°E , at the spatial resolution of $0.25^{\circ} \times 0.25^{\circ}$. Among the 15 variables included in MWF-ASCAT dataset, northward and eastward windspeed are utilized to capture the spirals in wind field.

Because ASCAT only records windspeed on water surface, the wind field can be cut off by small island [see Fig. 1(a)]. As reported by Xie et al. [13], this may negatively affect the cyclone detection results. Therefore, the wind field data within the small island (less than 4 pixels in either of the dimension) were interpolated with the windspeed data around. The bilinear interpolation method was applied to complete the spatial interpolation. The interpolated wind field is shown as Fig. 1(b).

2) *Precipitation Data*: Cyclone events usually bring strong rainfall in the cyclone wings, while low precipitation in the cyclone eyes. Nevertheless, it is unreliable to detect cyclone events by using precipitation data alone. Instead of that, precipitation can be applied as a side information with wind field. It can help

distinguish between cyclone and anticyclone turbulences since they have very different rainfall patterns.

In this article, the precipitation data is obtained from global precipitation measurement (GPM), which is provided by National Aeronautics and Space Administration and Japanese Aerospace Exploration Agency (JAXA). GPM derived precipitation calculation based on dual-frequency precipitation radar (13.6 GHz and 35.5 GHz). Upgraded from TRMM, GPM covers the entire global area at the spatial resolution of $0.1^\circ \times 0.1^\circ$.

3) *Data Preparation*: The input data of the cyclone detection model is constructed based on the two types of data components described previously. Generally, the integrated dataset consists of three layers: eastward windspeed from wind field data, northward windspeed from wind field data, and precipitation.

The three data layers need to be synchronized in terms of both spatial coverage and resolution. For spatial coverage, it is unrealistic to extent data coverage to the high-latitude area that is not covered in source data. Therefore, the minimum spatial coverage among the three data layers, which is 80°N - 80°S and 180°W - 0° - 180°E , was set as the spatial coverage of the integrated data, and any cross-boundary data were cut off in each data layer. For spatial resolution, it is also questionable to interpolate the data layers with low spatial resolution. Therefore, the lowest spatial resolution among the three data layers, which is $0.25^\circ \times 0.25^\circ$, was set as the spatial resolution of the integrated data. The spatial resolution of precipitation data needed to be resampled accordingly. Judging from the data fusion approach described previously, the spatial coverage and resolution of the integrated dataset are strongly affected by ‘‘cask effect,’’ which means that they are determined by the data layer that has the lowest spatial coverage and resolution.

It should be noted that the input data of each component need to be normalized before applied to the cyclone detection model, because the value of windspeed in m/s is usually much small than that of the precipitation in mm/h. If the data are directly fed to the model, the neural network may fail to evaluate the impacts of each component correctly. The overall data fusion process is shown as the flowchart in Fig. 2.

The time and locations of the cyclones were obtained as part from the cyclone and anticyclone dataset built by Xie et al. [13]. The latitude and longitude information of cyclones were verified with the hurricane data from Unisys Weather, and then transferred to the coordinates of integrated dataset, based on which the cyclones were labeled. We tried to balance the locations of cyclones: among the 1000 labelled cyclones, 469 of them were from the northern hemisphere, and 531 of them were from the southern hemisphere. The training data were randomly shuffled so that the cyclones were detected only through the integrated dataset but not the sequential patterns in time-series.

B. Model Structure

The cyclone detection model applied in this article was constructed based on an object detection algorithm of deep learning. Object detection is an important topic in the field of artificial intelligent algorithm and various models have been developed for this purpose. According to the model

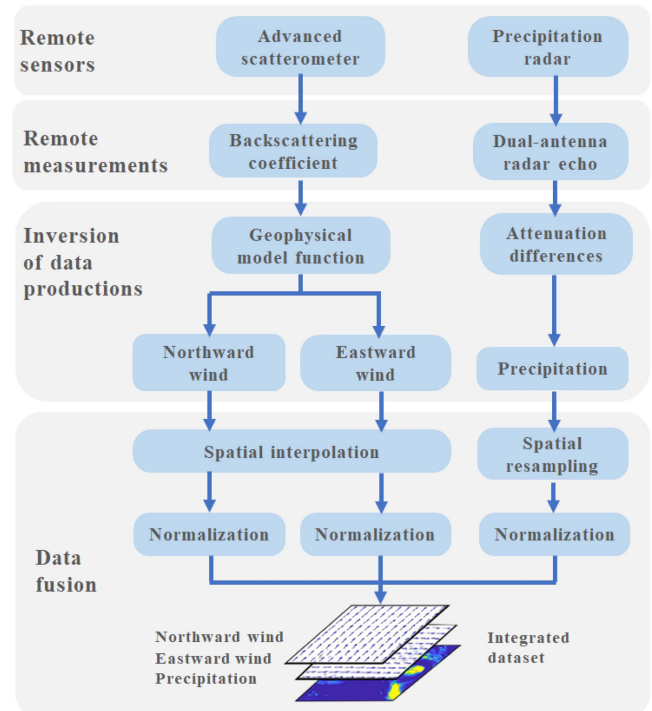


Fig. 2. Flowchart of the data fusion process.

structures, the deep-learning-based object detection models can be classified into two categories: 1) two-stage object detection, such as faster-RCNN [37] and SSP-Net [38], which usually consists of a regions proposal network (RPN) and a neural-network-based classifier; 2) one-stage object detection based on regression, such as YOLO [39] and SSD [40].

Since the cyclones usually appeared as small targets in the integrated dataset at the global-scale, their spatial features may be lost in the deep convolution operation. In order to solve this problem, feature pyramid network (FPN) was integrated with a modified faster-RCNN algorithm to construct the detection model. Specifically, the model consists of two parts: 1) a feature extraction and RPN built based on FPN that seeks for potential areas of cyclones within the feature maps generated under different levels of convolution operations and proposes regions of interests (ROI); 2) a ROI processor that calibrates the locations of proposed cyclone regions with fully-connected (FC) layer and bounding box regression. The overall structure of the faster-RCNN model applied in this article is shown as Fig. 3.

As shown in Fig. 3, 5 convolution layers and 5 pooling layers were applied on the integrated dataset and produced the feature maps, based on which FPN-RPN proposed candidate cyclone regions. The size of the convolutional kernel is 3×3 . The proposed regions were determined based on a fixed set of anchor sizes and positions. Because the shapes of cyclone regions are mostly close to a circle and can be enclosed in square regions, the anchor shape were set as squares. In terms of side lengths of the anchors, three types of anchor sizes were applied in the model according to the sizes of commonly witnessed cyclones on sea surface: 4, 8, and 16 pixels in integrated dataset, which represent 1° , 2° , and 4° on the earth surface.

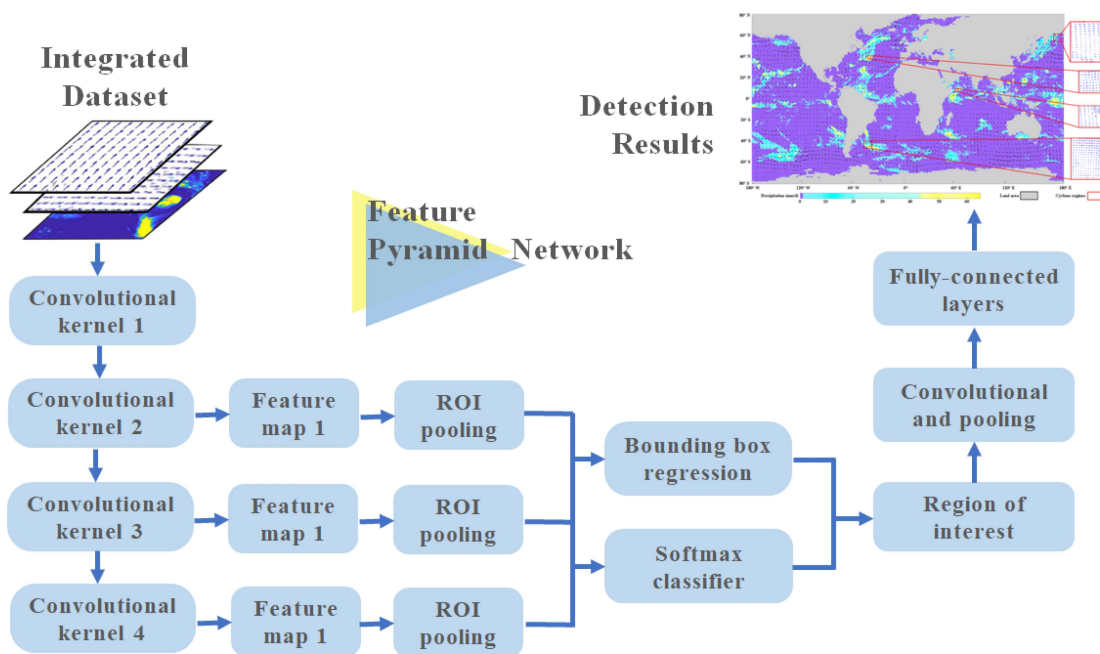


Fig. 3. Overall structure of the detection model.

With the deepening of the convolutional levels, more detailed information was learnt and the ability of feature expression was strengthened. However, if the targets to be detected are rather small (such as the cyclone regions at global-scale), the corresponding feature maps are likely to be over-compressed and lose some key information. As a result, it makes the cyclones difficult to be detected correctly. In this article, FPN was introduced to achieve multiscale feature fusion and object detection. FPN uses the pyramid structure of CNN hierarchical features and generates feature pyramids with strong semantics on all scales [41]. Its architecture is designed as a top-down structure with horizontal connections, which connect the shallow layer with high resolution and the deep layer with rich semantic information. As specifically shown in Fig. 3, the size of the feature maps becomes smaller after each convolution operation. The feature maps generated after each convolution operation are extracted and form a feature pyramid. In this way, the size of its feature map is increased while retaining the high-level semantic information. Thus, the feature pyramid with strong semantic information on all scales can be quickly constructed from a single input image of a single scale at small computational cost. The feature maps generated under level 2, 3, and 4 are used for the bounding box of cyclones generated under the size of 4, 8, and 16, respectively. Thus, the proposed bounding box with large size will tend to choose the feature level with the greater depth. In other words, the larger the target is, the lower the resolution and the more abstract the feature map will be selected for regression prediction. On the contrary, the regression prediction of small targets will be carried out in the high-resolution feature map. This can solve the problem of small target detection on faster-RCNN.

The proposed regions of cyclones are processed through ROI pooling and normalized as 5×5 feature maps, which are flattened

into feature vectors with the dimension of $1024 \times 1 \times 1$. Because there is only one class of target (cyclone) to be detected in the dataset, the Softmax classifier in the final classification layer of faster-RCNN is replaced by a bounding box regression that calibrates the locations of proposed cyclone regions. The FC layer and bounding box regression calibrate the location of the anchor based on these feature vectors. The FC layer consist of an input layer, three hidden layers, and an output layer.

Faster-RCNN model was intended to detect objects in RGB images. The integrated dataset constructed in this article also has a three-layers structure that is similar as RGB images. Nevertheless, if additional data were integrated into the dataset and further extent its dimension, the input size of feature extraction part would need to be modified in order to work with the dataset with extended dimension. Moreover, compared with regular faster-RCNN model, the cyclone detection model proposed in this article pruned a Softmax classification layer and its corresponding FC layer. As a result, the computational complexity is reduced and the model efficiency is improved.

C. Ablation Experiment

In order to evaluate the necessity of data fusion and determine the contribution of each data component on the detection result, an ablation experiment was designed and conducted. In addition to the model described previously that uses the data layers of wind field and precipitation, three additional contrasting models were designed in the ablation experiment by using only the wind field, precipitation, or windspeed from the input data. The detection accuracies using the three types of data were compared with that using the data fusion method.

It should be noted that when only one type of data in the integrated dataset, the number of data layers changes. As a

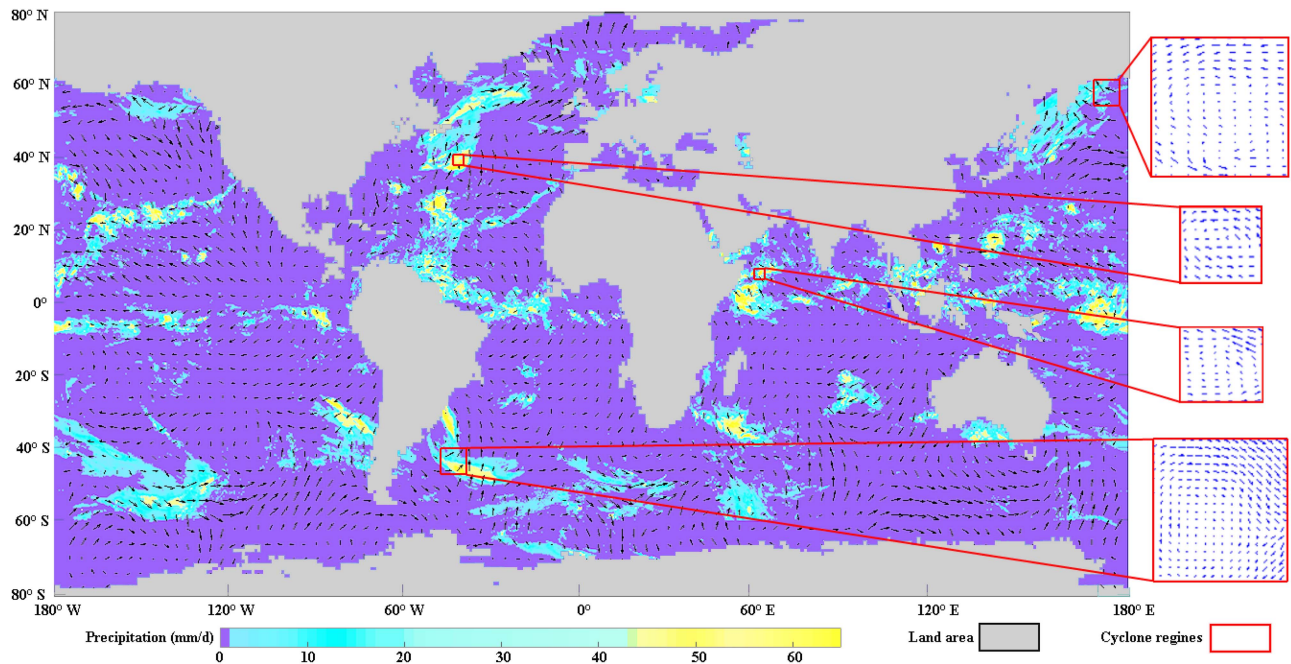


Fig. 4. Detection result on Feb. 25, 2020 at global scale.

result, the input size of the feature extractor needs to be modified accordingly. More specifically, the wind field data consist of two layers (northward wind and eastward wind), while the precipitation and windspeed data consist of only one layer and can be treated similar as the grayscale images. Transformer-based object detection model can be implemented with the similar RPN module, and thus could theoretically

D. Implementation Details

The models used in this article and ablation experiment were constructed and trained with Keras in the Tensorflow backend [42] and Python 3.6 environment. Rectified linear unit [43] was applied as the activation function between the convolutional and pooling layers. For the hyperparameters, the initial learning rate was set at 0.001, and reduced at a factor of 10 after 100 iterations. The maximum number of iterations is set at 10000. Nonmaximum suppression was applied in the classifier to decide the prediction, and the intersection-over-union thresholds of NMS are 0.8 and 0.2 for training and testing, respectively. The models were trained using the dataset built in the previous section. 70% of the wind field data were used for training, 10% of the data were used for validation, and 20% of the data were used for testing.

III. RESULTS

The performance of the detection model was tested using the wind field and precipitation data that collected from Feb. 25, 2020 to Mar. 5, 2020. Fig. 4 shows the cyclone detection results at global scale. The vectors in Fig. 4 represent for the magnitude and direction of windspeed. The background represents for the intensity of rainfall. The spatial resolution of the windspeed vectors in the insert panel is at $0.25^\circ \times 0.25^\circ$, while that of

the global vectors is resampled down to $4^\circ \times 4^\circ$. The spatial resolution for the rainfall intensity is the same as the input data ($0.25^\circ \times 0.25^\circ$). The results show that the model can detect cyclones at different latitude.

In order to compare the accuracy of the proposed model with those of the models for ablation experiment, the results are quantitatively evaluated by precision, recall, and F-measure, which are define as

$$\text{precision} = \frac{\text{TP}}{\text{TP} + \text{FP}} \quad (3)$$

$$\text{recall} = \frac{\text{TP}}{\text{TP} + \text{FN}} \quad (4)$$

$$F - \text{measure} = \frac{2 \cdot \text{precision} \cdot \text{recall}}{\text{precision} + \text{recall}} \quad (5)$$

where TP stand for true positive predictions, FP stand for false positive predictions, and FN stand for false negative predictions.

When the confidence threshold is set at a higher level, less object would be detected. This change would reduce the false alarms but increase the number of undetected objects, in other words, improving the precision at the cost of reducing the recall. By adjusting the confidence threshold and recording the corresponding precisions and recalls, a precision-recall (PR) curves can be plotted. Each point in the PR curve corresponds to a different threshold, and its value is determined by the corresponding precision and recall [44]. The area under the PR curve is a direct indicator of the models' accuracies, and has been widely-used to evaluate the performance of machine learning models [45]. The PR curves of the four models used in the ablation study is shown as Fig. 5. The results indicated that the detection model using the integrated dataset achieved accurate detection on cyclones, as the average precision (AP) values were

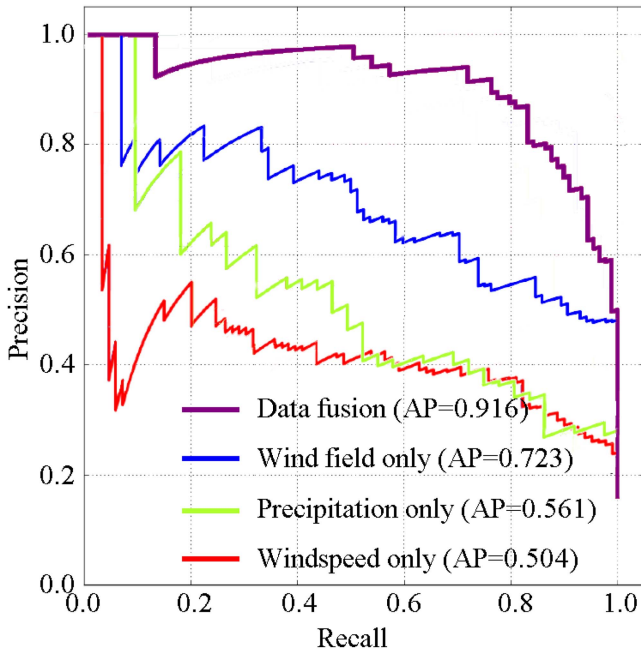


Fig. 5. PR curve of the cyclone detection results in the ablation study.

true label	(a)		(b)		(c)	
	cyclone	not detected	cyclone	not detected	cyclone	not detected
cyclone	152	9	127	34	104	57
non-cyclone	5	—	51	—	73	—
	cyclone		predicted label		cyclone	

Fig. 6. Confusion matrices of the detection results using different datasets. (a) Integrated dataset. (b) Wind field data only. (c) Precipitation data only.

TABLE I
PRECISIONS, RECALLS, AND F-MEASURES OF THE DETECTION RESULTS USING DIFFERENT DATASETS

DATASET	PRECISION	RECALL	F-MEASURE
INTEGRATED DATA	0.944	0.968	0.956
WIND FIELD DATA	0.788	0.713	0.749
PRECIPITATION DATA	0.646	0.623	0.634
WINDSPEED DATA	0.604	0.589	0.596

more than 0.9. The high precision and recall values are achieved with the confidence over 0.8. Therefore, the proposed regions with the confidence over 0.8 are preserved for the model training. However, the APs for the classification models that only uses wind field, precipitation, or windspeed were significantly lower than that using the integrated data. The confusion matrices of the detection results are shown in Fig. 6. Based on the confusion matrices, the accuracies can be calculated in Table I.

As shown in the confusion matrix (see Fig. 6), the proposed model using the data fusion approach provided the cyclone detection results with smallest number of FN and FP predictions. It also achieved the highest F-measure of over 95%. The model using only wind field data resulted in less FN and FP predictions, and thus higher accuracies (about 75%) than that using only

TABLE II
PRECISIONS, RECALLS, AND F-MEASURES OF THE DETECTION RESULTS USING DIFFERENT MODELS

DATASET	PRECISION	RECALL	F-MEASURE
FPN+FASTER-RCNN	0.944	0.968	0.956
FASTER-RCNN	0.901	0.882	0.891
YOLOV4	0.928	0.906	0.917

precipitation data (about 63%) or windspeed data (60%). But all of these three models achieved lower detection accuracies than that of the proposed model using the data fusion approach.

A comparison study was also conducted by replacing the classifier in the proposed model with other existing models including Faster-RCNN [37] and YOLOv4 [39]. It can be seen from the comparison results shown in Table II that the proposed FPN+faster-RCNN model achieved higher detection accuracies than existing models. Compared with the object detection model proposed in [37] and [39], the proposed model includes the FPN module that can effectively recognize the small targets. Considering the size of cyclones at the global scale, integrating FPN in the detection model should be an appropriate improvement. This can also be verified from the comparison results shown in Table II.

IV. DISCUSSION

A. Accuracy Analysis on the Ablation Experiment

As indicated by the cyclone detection results (see Fig. 4), the proposed FPN+faster-RCNN model can effectively identify cyclones through the data fusion method. According to the detection results using three different datasets (see Table I and Fig. 5), the detection model using the data fusion approach can achieve significantly better performance than those using single type of data. Moreover, the detection model using wind field data provide better prediction than that using precipitation data. These results are also confirmed by the PR curves (see Fig. 5).

It should be noted that if the cyclone locates at the boundary of the integrated dataset, part of the cyclone would be cut off by the 180° meridian or 80° parallel and the model would fail to detect it. For the cyclones cut off by the 180° meridian, the problem may be solved by adding a duplicating padding of the dataset on the other boundary (e.g., 2° to 4° in longitude). However, this would not solve the cyclones cut off by the 80° parallel, since the polar area are not covered in ASCAT data and affected by the “cask effect”. With the appropriate data coverage, the model should also work for the cyclone detection in polar area.

Compared with the detection model using the data fusion approach, the model that only used wind field data ended up in much lower precision (see Table I), which indicated more false alarms. According to a detailed examination on the false alarms, this was because that the model was not able to distinguish between the cyclones and anticyclones at global scale very well, as they rotate in the different direction in north- and south-hemisphere. This problem can be solved through data fusion by introducing precipitation data, since cyclone, and anticyclone events have very different rainfall condition. The model that only

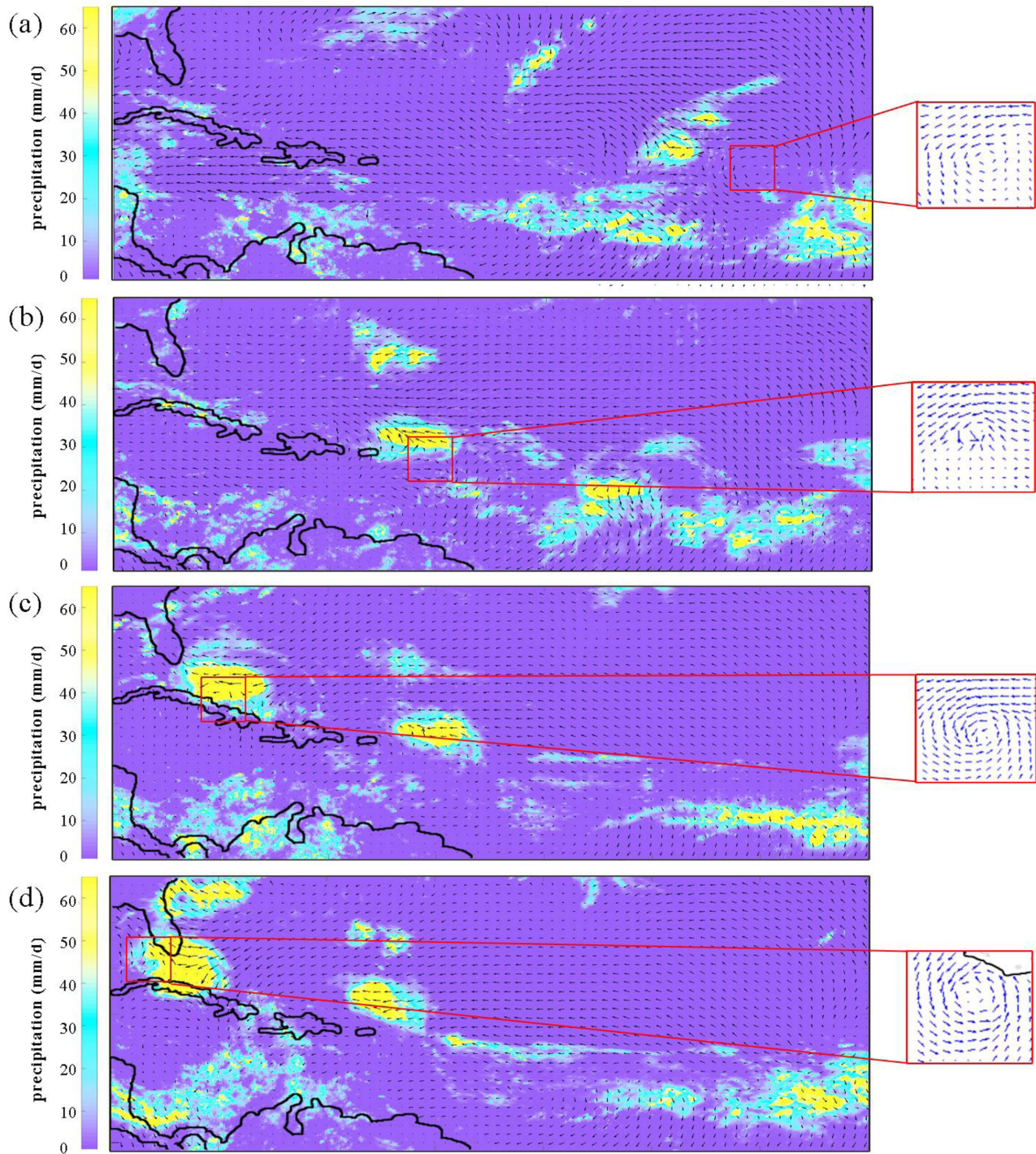


Fig. 7. Tracking the path of Hurricane Irma in the time-series data. (a) Aug. 31, 2017. (b) Sep. 5, 2017. (c) Sep. 8, 2017. (d) Sep. 9, 2017.

used the windspeed data provided detection results lower than that using only wind field data because it lacks the information in wind direct, which helps identify the cyclones through their vortex structures. The model that only used precipitation data was also not able to provided very accurate prediction, since high rainfall intensity could be related to various weather conditions besides cyclone events. Furthermore, because the detection results using wind field data were more accurate than that using precipitation data, wind field data were likely to have higher

contribution in the cyclone detection process of data fusion approach than precipitation data.

B. Application Areas and Future Studies

A direct application of the proposed data fusion method would be tracking the cyclone path. By processing the integrated dataset in temporal sequence with the cyclone detection model, the locational information of the cyclones can be obtained through

the proposed regions and the movement of a cyclone can be captured by the model. For example, we attempted to track the path of Hurricane Irma that occurred in September 2017 with the proposed model. The time-series results are shown sequentially in Fig. 7. The spatial resolution of the windspeed vectors in the insert panel is at $0.25^\circ \times 0.25^\circ$, while that of the regional vectors is resampled down to $1^\circ \times 1^\circ$. The spatial resolution for the rainfall intensity is set as the raw data ($0.1^\circ \times 0.1^\circ$). As indicated in the results, the model was able to detect Hurricane Irma and track its moving path, which started from the west Atlantic Ocean [see Fig. 7(a)], passed over Cuba [see Fig. 7(b) and (c)], and turned north toward Florida, United States [see Fig. 7(d)].

It should be noted that the proposed model has not been developed into a completed cyclone tracking model yet for the following reasons: 1) For the purpose of cyclone tracking, it is usually important to determine the locations of cyclone eyes, while the proposed model only indicated the cyclone regions. The most straightforward way to locate the cyclone eyes is to make the centers of the proposed regions as the location of the cyclone eyes. This may not be accurate though, since the wind fields of the cyclones could be asymmetric; 2) The spatial resolution of the integrated dataset is not fine enough to precisely determine the locations of cyclone eyes. As stated previously in the methodology part, the spatial resolution of the integrated dataset is influenced by “cask effect”. Thus, in order to solve this problem, the data component with the lowest spatial resolution needs to be improved. This problem could be solved through the future development of remote sensing technology; 3) ASCAT and GPM data are derived from polar satellites that provide two passes in a day. However, cyclones are moving phenomena, of which the spatial coverage may not be correctly indicated on daily-averaged data. Geostationary satellites collect continuous observations for cyclone tracking, but with lower accuracy. Therefore, the proposed model can be applied as an additional validation of cyclone tracking using geostationary satellite.

For the same reasons, the proposed approach can be more appropriately applied for the census of cyclone occurrences in large spatial and temporal scales. Such studies usually do not require precise location of the cyclone eyes. As a global-scale, fully-automatic cyclone detection model with high efficiency and accuracy, the proposed data fusion approach can be applied to construct an archive of historical occurrences of cyclone events in large temporal and spatial scale, and propel further studies on the patterns of cyclone occurrences.

A direct application of the proposed data fusion method would be tracking the cyclone path. By processing the integrated dataset in temporal sequence with the cyclone detection model, the locational information of the cyclones can be obtained through the proposed regions and the movement of a cyclone can be captured by the model. For example, we attempted to track the path of Hurricane Irma that occurred in September 2017 with the proposed model. The time-series results are shown sequentially in Fig. 7. The spatial resolution of the windspeed vectors in the insert panel is at $0.25^\circ \times 0.25^\circ$, while that of the regional vectors is resampled down to $1^\circ \times 1^\circ$. The spatial resolution for the rainfall intensity is set as the raw data ($0.1^\circ \times 0.1^\circ$). As

indicated in the results, the model was able to detect Hurricane Irma and track its moving path, which started from the west Atlantic Ocean [see Fig. 7(a)], passed over Cuba [see Fig. 7(b) and (c)], and turned north toward Florida, United States [see Fig. 7(d)].

Besides the data fusion approaches, we envision an improvement on the performance of cyclone detection model as the trends of future studies, and there are at least two ways to pursue that. The first approach focuses on the configuration of neural network structure. For instance, the lately-proposed transformer-based object detection, which was built on object queries rather than the bounding boxes used in the faster-RCNN or YOLO [46], may be an alternative detector to process the integrated dataset. Transformer-based object detection model can be implemented with the similar RPN module [47], and thus could theoretically be applied to detect small cyclone targets at the global scale. However, considering the problem of tedious training time and low running efficiency in the transformer-based object detection model [48], its feasibility of global cyclone detection still needs to be further verified. The other approach would be the integration of physic model and artificial neural network, which has drawn the attentions of researches in different application fields [49]. For the purpose of cyclone detection, the OW method may be combined with the deep learning model where the distribution of OWZP operator could provide additional information that imply the exist of cyclones.

V. CONCLUSION

A data fusion approach for global scale cyclone detection is proposed using deep-learning-based object detection algorithm. Wind field vectors derived from ASCAT scatterometer and rainfall intensity derived from precipitation radar are combined and form an integrated dataset for model training and testing. The experiment results showed that the detection model using the data fusion approach was able to provide significantly more accurate detection than those using single types of data. This fact indicated the necessity of data fusion. Furthermore, according to the results of ablation experiment, the wind field data seemed to have higher contribution than precipitation data for the cyclone detection model applied in this article.

The limitations and potential applications of the detection model are also discussed in the article. The spatial resolution of the dataset is affected by “cask effect”. In other words, the spatial resolution of the dataset is determined by the data layer with the lowest spatial resolution. Therefore, it may not be able to accurately determine the locations of cyclone eyes according to the current spatial resolution of remote sensing data. However, by developing a fully-automatic cyclone detection model with data fusion approach, this article is expected to promote the researches on the cyclone occurrences and climate patterns, as well as remote sensing data fusion methods.

ACKNOWLEDGMENT

The authors would like to thank the European Remote Sensing program of the European Space Agency for providing free satellite data, like to thank National Aeronautics and Space

Administration and Japanese Aerospace Exploration Agency for providing precipitation data, and the National Centers for Environmental Prediction for providing free hurricane and storm data, like to thank Q. Yu, Z. Ma, and W. Zheng from Dalian Maritime University for their help in preparing the training dataset, and also like to thank X. Cheng for optimizing the artworks.

REFERENCES

- [1] T. P. Barnett, "Variations in near global sea level pressure," *J. Atmospheric Sci.*, vol. 42, no. 5, pp. 478–501, 1985.
- [2] M. R. Sinclair, "Objective identification of cyclones and their circulation intensity and climatology," *Weather Forecasting*, vol. 12, pp. 595–612, 1997.
- [3] I. Rudeva and S. K. Gulev, "Climatology of cyclone size characteristics and their changes during the cyclone life cycle," *Monthly Weather Rev.*, vol. 135, pp. 2568–2587, 2007.
- [4] I. Simmonds, C. Burke, and K. Keay, "Arctic climate change as manifest in cyclone behavior," *J. Climate*, vol. 21, no. 22, pp. 5777–5796, 2008.
- [5] J. Hanley and R. Caballero, "Objective identification and tracking of multicentre cyclones in the ERA-Interim reanalysis dataset," *Quart. J. Roy. Meteorological Soc.*, vol. 138, no. 664, pp. 612–625, 2012.
- [6] A. Okubo, "Horizontal dispersion of floatable particles in the vicinity of velocity singularities such as convergences," *Deep Sea Res. Oceanogr. Abstr.*, vol. 17, no. 3, pp. 445–454, 1970.
- [7] J. Weiss, "The dynamics of enstrophy transfer in two-dimensional hydrodynamics," *Physica D*, vol. 48, no. 2/3, pp. 273–294, 1991.
- [8] M. Inatsu, "The neighbor enclosed area tracking algorithm for extratropical wintertime cyclones," *Atmos. Sci. Lett.*, vol. 10, pp. 267–272, 2009.
- [9] J. Zou, M. Lin, X. Xie, S. Lang, and S. Cui, "Automated typhoon identification from QuikSCAT wind data," in *Proc. IEEE Int. Geosci. Remote Sens. Symp.*, 2010, pp. 4158–4161.
- [10] K. J. Tory, R. A. Dare, N. E. Davidson, J. L. McBride, and S. S. Chand, "The importance of low-deformation vorticity in tropical cyclone formation," *Atmos. Chem. Phys. Discuss.*, vol. 12, no. 4, pp. 17539–17581, 2012.
- [11] K. J. Tory, S. S. Chand, R. A. Dare, and J. L. McBride, "The development and assessment of a model-, grid-, and basin-independent tropical cyclone detection scheme," *J. Climate*, vol. 26, no. 15, pp. 5493–5507, Aug. 2013.
- [12] K. J. Tory, S. S. Chand, R. A. Dare, and J. L. McBride, "An assessment of a model-, grid-, and basin-independent tropical cyclone detection scheme in selected CMIP3 global climate models," *J. Climate*, vol. 26, no. 15, pp. 5508–5522, 2013.
- [13] M. Xie, Y. Li, and K. Cao, "Global cyclone and anticyclone detection model based on remotely sensed wind field and deep learning," *Remote Sens.*, vol. 12, no. 19, 2020, Art. no. 3111.
- [14] R. S. T. Lee and J. N. K. Liu, "Tropical cyclone identification and tracking system using integrated neural oscillatory elastic graph matching and hybrid RBF network track mining techniques," *IEEE Trans. Neural Netw.*, vol. 11, no. 3, pp. 680–689, May 2000.
- [15] N. Jaiswal and C. M. Kishitawal, "Automatic determination of center of tropical cyclone in satellite-generated IR images," *IEEE Geosci. Remote Sens. Lett.*, vol. 8, no. 3, pp. 460–463, May 2011.
- [16] N. Jaiswal and C. M. Kishitawal, "Objective detection of center of tropical cyclone in remotely sensed infrared images," *IEEE J. Sel. Topics Appl. Earth Observ. Remote Sens.*, vol. 6, no. 2, pp. 1031–1035, Apr. 2013.
- [17] J. Liu, C. Liu, B. Wang, and D. Qin, "A novel algorithm for detecting center of tropical cyclone in satellite infrared images," in *Proc. IEEE Int. Geosci. Remote Sens. Symp.*, 2015, pp. 917–920.
- [18] X. Xu, C. Liu, and J. Liu, "A novel algorithm for the objective detection of tropical cyclone centres using infrared satellite images," *Remote Sens. Lett.*, vol. 7, no. 6, pp. 541–550, 2016.
- [19] S. Shakya, S. Kumar, and M. Goswami, "Deep learning algorithm for satellite imaging based cyclone detection," *IEEE J. Sel. Topics Appl. Earth Observ. Remote Sens.*, vol. 13, pp. 827–839, Jan. 2020.
- [20] K. V. Khlopenkov and K. M. Bedka, "Development of pattern recognition algorithms to detect intense convective storms from multispectral satellite imagery," in *Proc. IEEE Int. Geosci. Remote Sens. Symp.*, 2018, pp. 4850–4852.
- [21] S. Shah et al., "Automatic storm(s) identification in high resolution, short range, X-band radar images," in *Proc. IEEE Int. Conf. Electromagn. Adv. Appl.*, 2013, pp. 945–948.
- [22] C. Kumler-Bonfanti, J. Stewart, D. Hall, and M. Govett, "Tropical and extratropical cyclone detection using deep learning," *J. Appl. Meteorol. Climate*, vol. 59, no. 12, pp. 1971–1985, 2020.
- [23] M. Pineros, E. Ritchie, and J. Tyo, "Objective measures of tropical cyclone structure and intensity change from remotely sensed infrared image data," *IEEE Trans. Geosci. Remote Sens.*, vol. 46, no. 11, pp. 3574–3580, Nov. 2008.
- [24] M. Pineros, E. Ritchie, and J. Tyo, "Estimating tropical cyclone intensity from infrared image data," *Weather Forecasting*, vol. 26, pp. 690–698, 2011.
- [25] E. Ritchie, G. Valliere-Kelley, M. Piñeros, and J. Tyo, "Tropical cyclone intensity estimation in the north Atlantic basin using an improved deviation angle variance technique," *Weather Forecasting*, vol. 27, pp. 1264–1277, 2012.
- [26] E. Ritchie, K. Wood, O. Rodríguez-Herrera, M. Piñeros, and J. Tyo, "Satellite-derived tropical cyclone intensity in the north pacific ocean using the deviation-angle variance technique," *Weather Forecasting*, vol. 29, pp. 505–516, 2014.
- [27] T. Olander and C. Velden, "The advanced Dvorak technique: Continued development of an objective scheme to estimate tropical cyclone intensity using geostationary infrared satellite imagery," *Weather Forecasting*, vol. 22, pp. 287–298, 2007.
- [28] T. Olander and C. Velden, "The advanced dvorak technique (ADT) for estimating tropical cyclone intensity: Update and new capabilities," *Weather Forecasting*, vol. 34, pp. 905–922, 2019.
- [29] A. Wimmers, C. Velden, and J. Cossuth, "Using deep learning to estimate tropical cyclone intensity from satellite passive microwave imagery," *Monthly Weather Rev.*, vol. 147, pp. 2261–2282, 2019.
- [30] J. Lee, J. Im, D. Cha, H. Park, and S. Sim, "Tropical cyclone intensity estimation using multi-dimensional convolutional neural networks from geostationary satellite data," *Remote Sens.*, vol. 12, no. 1, 2019, Art. no. 108.
- [31] M. Maskey et al., "Deepti: Deep-learning-based tropical cyclone intensity estimation system," *IEEE J. Sel. Top. Appl. Earth Observ. Remote Sens.*, vol. 13, pp. 4271–4281, Jul. 2020.
- [32] S. S. Ho and A. Talukder, "Automated cyclone identification from remote QuikSCAT satellite data," in *Proc. IEEE Aerosp. Conf.*, 2008, pp. 1–9.
- [33] S. S. Ho and A. Talukder, "Automated cyclone tracking using multiple remote satellite data via knowledge transfer," in *Proc. IEEE Aerosp. Conf.*, 2009, pp. 1–7.
- [34] S. S. Ho and A. Talukder, "Automated cyclone discovery and tracking using multiple knowledge sharing in multiple heterogeneous satellite data," in *Proc. Int. Conf. Knowl. Discov. Data Min.*, 2009, pp. 928–936.
- [35] K. Warunsin and O. Chitsobhuk, "Storm eye identification using fuzzy inference system," *Int. J. Innov. Comput. Inf. Control.*, vol. 12, pp. 1333–1349, 2016.
- [36] A. Murata, S. I. Watanabe, H. Sasaki, H. Kawase, and M. Nosaka, "The development of a resolution-independent tropical cyclone detection scheme for high-resolution climate model simulations," *J. Meteorol. Soc. Jpn.*, vol. 97, no. 2, pp. 519–531, 2019.
- [37] S. Ren, K. He, R. Girshick, and J. Sun, "Faster-RCNN: Towards real-time object detection with region proposal networks," in *Proc. Neural Inf. Process. Syst.*, 2015, pp. 265–283.
- [38] K. He, X. Zhang, S. Ren, and J. Sun, "Spatial pyramid pooling in deep convolutional networks for visual recognition," *IEEE Trans. Pattern Anal. Mach. Intell.*, vol. 37, no. 9, pp. 1904–1916, Sep. 2015.
- [39] J. Redmon, S. Divvala, R. Girshick, and A. Farhadi, "You only look once: Unified, real-time object detection," in *Proc. IEEE Conf. Comput. Vis. Pattern Recognit.*, 2016, pp. 779–788.
- [40] W. Liu et al., "SSD: Single shot multibox detector," in *Proc. Eur. Conf. Comput. Vis.*, 2016, pp. 21–37.
- [41] T. -Y. Lin, P. Dollár, R. Girshick, K. He, B. Hariharan, and S. Belongie, "Feature pyramid networks for object detection," in *Proc. IEEE Conf. Comput. Vis. Pattern Recognit.*, 2017, pp. 936–944.
- [42] M. Abadi et al., "TensorFlow: A system for large-scale machine learning," in *Proc. 12th USENIX Symp. Operating Syst. Des. Implementation*, 2016, pp. 265–283.
- [43] V. Nair and G. E. Hinton, "Rectified linear units improve restricted Boltzmann machines," in *Proc. Int. Conf. Mach. Learn.*, 2010, pp. 807–814.
- [44] D. M. W. Powers, "Evaluation: From precision, recall and F-measure to ROC, informedness, markedness and correlation," *J. Mach. Learn. Technol.*, vol. 2, no. 1, pp. 37–63, Feb. 2011.
- [45] A. Tharwat, "Classification assessment methods," *Appl. Comput. Info.*, vol. 17, no. 1, pp. 168–192, 2020.

- [46] H. Vaidwan, N. Seth, A. S. Parihar, and K. Singh, "A study on transformer-based object detection," in *Proc. Int. Conf. Intell. Technol.*, 2021, pp. 1–6.
- [47] C. Samplawski and B. M. Marlin, "Towards transformer-based real-time object detection at the edge: A benchmarking study," in *Proc. IEEE Mil. Commun. Conf.*, 2021, pp. 898–903.
- [48] E. Arkin, N. Yadikar, Y. Muhtar, and K. Ubul, "A survey of object detection based on CNN and transformer," in *Proc. 2nd Int. Conf. Pattern Recognit. Mach. Learn.*, 2021, pp. 99–108.
- [49] Q. Yuan et al., "Deep learning in environmental remote sensing: Achievements and challenges," *Remote Sens. Environ.*, vol. 241, 2020, Art. no. 111716.



Ming Xie (Member, IEEE) received the B.S. degree in physical geography from Nanjing University, Nanjing, China, in 2008, the M.S. degree in coastal geology from the University of South Florida, Tampa, FL, USA, in 2015, and the Ph.D. degrees in geographic information science from the University of South Florida, Tampa, FL, USA, in 2019.

He is currently an Instructor with Navigation College, Dalian Maritime University, China. He is aiming at the cross-boundary researches between advanced machine learning method and modern remote sensing technology. His current research interests include the applications of advanced machine learning method in remote sensing data processing and object detection, as well as the application of GIS and remote sensing technology in coastal environment and transportation.



Ying Li received the Ph.D. degree in geographic information science from Tohoku University, Miyagi, Japan, in 1996.

She is currently a Professor with Navigation College, Dalian Maritime University, China, and the Dean of Environmental Information Institute, Dalian Maritime University. Under the authorization of ESRI, she set up teaching and research center of ArcGIS in Dalian Maritime University. She is committed to the research and application of GIS and remote sensing technology in oceanic environment and maritime transportation, as well as the detection technology of oil pollution.

Dr. Li invention of oil spill detection instrument based on remote sensor is awarded as the second prize of National Technological Invention Award of China.



Shuang Dong received the B.Sc. degree in navigation science from Dalian Oceanography University, Dalian, China, in 2016, and the M.S. degree in transportation information science from Dalian Maritime University, Dalian, China, in 2022. He is currently working towards the Ph.D. degree in transportation information science from Dalian Maritime University, Dalian, China.

His current research interests include the interpretation of ocean remote sensing data, and the applications of remote sensing technology in marine

transportation.